

SleepMaMi: A Universal Sleep Foundation Model for Integrating Macro- and Micro-structures

Keondo Park¹ Younghoon Na² Yourim Choi¹ Hyunwoo Ryu¹
 Hyun-Woo Shin^{2,3,4} Hyung-Sin Kim¹

Abstract

While the shift toward unified foundation models has revolutionized many deep learning domains, sleep medicine remains largely restricted to task-specific models that focus on localized micro-structure features. These approaches often neglect the rich, multi-modal context of Polysomnography (PSG) and fail to capture the global macro-structure of a full night's sleep. To address this, we introduce *SleepMaMi*, a Sleep Foundation Model engineered to master both hour-long sleep architectures and fine-grained signal morphologies. Our framework utilizes a hierarchical dual-encoder design: a Macro-Encoder to model full-night temporal dependencies and a Micro-Encoder to capture short-term characteristics from biosignals. Macro-Encoder is trained via *Demographic-Guided Contrastive Learning*, which aligns overnight sleep patterns with objective subject metadata, such as age, sex and BMI to refine global representations. Micro-Encoder is optimized via a hybrid Masked Autoencoder (MAE) and multi-modal contrastive objective. Pre-trained on a massive corpus of >20,000 PSG recordings (158K hours), *SleepMaMi* outperforms existing foundation models across a diverse suite of downstream tasks, demonstrating superior generalizability and label-efficient adaptation for clinical sleep analysis.

1. Introduction

Sleep occupies approximately one-third of the human lifespan and is a fundamental pillar of systemic health. Given its critical role, extensive research has been dedicated to decoding the complex physiological processes that govern sleep and addressing the myriad sleep disorders affecting hundreds of millions of population worldwide (Benjafield et al., 2019). The clinical gold standard for these investigations is Polysomnography (PSG), a multi-modal diagnostic tool that captures a diverse array of biosignals, including electroencephalogram (EEG), electrooculogram (EOG), electrocardiogram (ECG), electromyogram (EMG), and respiratory signals.

Comprehensive sleep analysis necessitates a dual-perspective approach. It requires the examination of sleep micro-structure — high-frequency physiological features observable within few seconds — and sleep macro-structure — the global organization of sleep stages and cycles across a full-night recording. However, analyzing PSG is not a standard long-sequence modeling problem. It requires integrating heterogeneous modalities with varying sampling rates while capturing both transient micro-events and hour-scale macro-architecture within a single representation. (Phan et al., 2019)

The labor-intensive nature of manual PSG scoring has catalyzed the development of deep learning models for automated analysis. However, existing literature remains largely fragmented. Most current approaches are task-specific (e.g., sleep staging) and depend on supervised approaches (Park et al., 2025; Retamales et al., 2024). While these models achieve impressive performance within their narrow domains, they lack the generalized representations necessary for cross-task transfer and depend on expert-scored labels (Perslev et al., 2021), lacking scalability and exposing the models to annotation noise (Danker-Hopfe et al., 2004; 2009; Guillot et al., 2020). Crucially, clinical research has established that sleep macro-architecture serves as a vital biomarker for long-term health outcomes and disease prognosis (Mander et al., 2017; Blackwell et al., 2011). Despite this clinical evidence, a significant gap remains in modeling macro-structural dynamics, which limits the appli-

¹Graduate School of Data Science, Seoul National University, Seoul, South Korea ²Obstructive Upper Airway Research (OUaR) Laboratory, Department of Pharmacology, Seoul National University College of Medicine, Seoul, Republic of Korea ³OUaR LaB, Inc, Seoul, Republic of Korea ⁴Department of Otorhinolaryngology-Head and Neck Surgery, Seoul National University Hospital, Seoul, Republic of Korea. Correspondence to: Hyun-Woo Shin <charlie@snu.ac.kr>, Hyung-Sin Kim <hyungkim@snu.ac.kr>.

cability of these models for subject-level clinical diagnosis and long-term health prediction.

To bridge these gaps, we propose *SleepMaMi*, a unified Sleep Foundation Model designed to master both micro- and macro-structural sleep representations (Figure 1). Pre-trained on 20,964 PSG recordings (158,028 hours), *SleepMaMi* shows strong generalizability and label-efficient adaptation to downstream tasks. *SleepMaMi* adopts a hierarchical architecture comprising two specialized components: the **Micro-Encoder** utilizes a shared-private transformer architecture to capture the idiosyncratic patterns of individual modalities alongside their cross-modal correlations. It is optimized via a hybrid strategy of masked autoencoding (MAE) (He et al., 2022) and contrastive learning (CL) (Oord et al., 2018) to learn robust, fine-grained latent features. To capture global context, the **Macro-Encoder** processes full-night sequences using a *Demographic-Guided Contrastive Learning* objective. By aligning sequence-level embeddings with objective demographic metadata (e.g., age, sex and BMI), the model learns to represent the normative and pathological trajectories of sleep macrostructure.

Our primary contributions are summarized as follows:

- We introduce *SleepMaMi*, the first foundation model that explicitly encodes both micro- and macro-structural sleep features, enabling a range of applications from second-level segmentation to subject-level disease prediction.
- We propose a novel training paradigm for biosignals that combines MAE-based reconstruction with multi-modal contrastive alignment, ensuring both signal-specific fidelity and cross-modal consistency.
- We introduce *Demographic-Guided Contrastive Learning*, an objective, metadata-driven pre-training strategy that optimizes long-sequence modeling without the need for subjective manual annotations, effectively capturing global sleep architecture.
- We demonstrate that *SleepMaMi* significantly outperforms existing foundation models across a diverse suite of benchmarks, proving its robustness in both local and global temporal tasks.

2. Related Work

2.1. Neural Networks for PSG Analysis

The vast amount of analysis required to understand PSG has drawn a great amount of attention towards using neural networks for the analysis. One of the most common task is sleep scoring. Various methods have been proposed to address sleep scoring. Early studies used Convolutional Neural Networks (CNN) (Supratak et al., 2017; Perslev et al., 2021), Recurrent Neural Networks (RNN) (Phan et al., 2019) for sleep scoring. Transformer-based architectures (Phan et al., 2022; Lee et al., 2024; Park et al.,

2025) have achieved good predictive performance. While these works have achieved good sleep scoring results, most of them solely rely on EEG and cannot be used for other downstream tasks than sleep staging. Other tasks, such as sleep apnea detection (Levy et al., 2023; Retamales et al., 2024) and age estimation (Sun et al., 2019; Brink-Kjaer et al., 2022), have also been proposed, but these works can only be used for certain target tasks and lack generalizability. Sleep foundation models are proposed to make use of the full potentials included in the multitude of signals from PSG to be used for diverse downstream tasks. SleepFM (Thapa et al., 2024) pioneered this movement to utilize the full range of signals to be used for various downstream tasks including sleep scoring, apnea detection and age/sex estimation. The subsequent work (Thapa et al., 2026) expanded its coverage to disease prediction. Most prior works have focused solely on sleep micro-structure or macro-structure, but *SleepMaMi* encompasses both aspects of sleep, showing great performance on several downstream tasks ranging from sleep apnea segmentation to disease prediction.

2.2. Time-series Foundation Model

Time series data have been studied for decades. While statistical models have been mainly used for its analysis, deep learning models recently have shown superior performance. For more general purpose use across a myriad of different types of data, time-series foundation models have been proposed. TimesFM (Das et al., 2024) proposes decoder-only foundation model pretrained on large corpus of time-series data. Moirai (Woo et al., 2024) proposed cross-frequency and any-variate time series foundation model. But these models are limited to time-series forecasting and cannot be directly utilized to sleep downstream tasks, which are mainly classification tasks. MO-MENT (Goswami et al., 2024) shows MAE-based pretraining on large-scale data is effective for diverse time-series downstream tasks. UniTS (Gao et al., 2024) proposes task tokenization and unified mask reconstruction to make a generalizable foundation model.

While these models could also be used for PSG analysis, its performance is suboptimal as presented in the Experiments section. *SleepMaMi* has a deep understanding of the characteristics of sleep data, and shows superior performance on various tasks.

3. *SleepMaMi*

SleepMaMi consists of Micro- and Macro- encoders. Both encoders are pretrained on large-scale PSG data with self-supervised learning. As shown from previous studies (Park et al., 2025), PSG scoring inconsistency exists within a dataset and between different datasets due to inter-scorer variability (Danker-Hopfe et al., 2004) or guideline up-

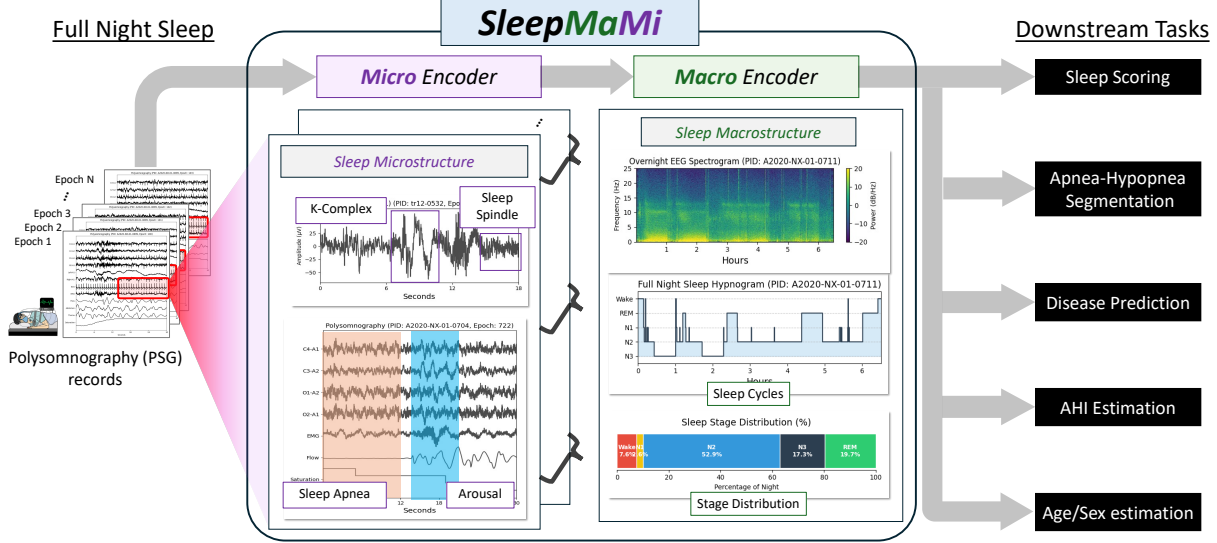


Figure 1. Overview of SleepMaMi. Full-night PSG recordings are processed through a hierarchical dual-encoder architecture. The Micro-Encoder captures short-term physiological patterns such as K-complexes, sleep spindles, and respiratory events, while the Macro-Encoder models global sleep architecture including sleep cycles and stage distributions across the entire recording. This design supports diverse downstream tasks ranging from fine-grained event segmentation to subject-level clinical outcomes.

dates (Berry, 2012; Berry et al., 2017). Independence from scored labels helps *SleepMaMi* to obtain generalizable embeddings and achieve scalability across diverse datasets.

3.1. Micro-Encoder

Micro-Encoder architecture The Micro-Encoder is designed to map multi-modal raw biosignals into a latent embedding space, enabling the model to capture fine-grained sleep micro-structure. The overall architecture is described in Figure 2. Raw signals are first partitioned into a sequence of patches through modality-specific convolutional embedding layers. These layers accommodate modality-dependent signal characteristics while preserving local temporal dependencies.

The resulting patch sequences are processed by a bifurcated architecture consisting of **modality-private encoders** and a single **modality-shared encoder**. The private encoders specialize in modeling patterns intrinsic to each signal type (e.g., rhythmic oscillations in EEG or QRS complexes in ECG), whereas the shared encoder focuses on extracting modality-invariant physiological features and cross-modal correlations.

Both private and shared encoders are built upon a Transformer backbone (Vaswani et al., 2017) enhanced with modern architectural refinements to improve training stability and representational capacity. Specifically, we adopt rotary positional embeddings (Su et al., 2024), a pre-normalization scheme (Xiong et al., 2020) using RMSNorm (Zhang & Senrich, 2019), and SwiGLU activation functions (Shazeer, 2020) within the feed-forward layers. To further enhance scalability and specialization, the shared encoder employs

a Mixture-of-Experts (MoE) architecture (Lepikhin et al., 2020), allowing different experts to selectively model distinct physiological patterns and inter-modal interactions.

The private encoders follow a hierarchical design to enable efficient temporal abstraction. At lower layers, individual patches are processed independently within each private encoder. Subsequently, every M consecutive patches are merged into a single higher-level representation, which is then forwarded both to the next private encoder layer and to the shared encoder. The merged representations from all private encoders are concatenated and jointly processed by the shared encoder, facilitating the modeling of complex inter-modal relationships. Although concatenation increases the effective input dimensionality with the number of modalities, the hierarchical merging substantially reduces the overall sequence length, maintaining computational efficiency.

To integrate information from the dual streams, the output of the shared encoder is re-partitioned by modality and fused with the corresponding private encoder representations via cross-attention. The resulting fused embeddings are subsequently up-sampled and passed to a decoder that reconstructs the masked segments of the original biosignals.

The hierarchical merging mechanism requires careful coordination with the masking strategy to preserve temporal alignment. To ensure that each merged representation corresponds to a consistent temporal span, we employ a structured masking scheme in which masks are applied at fixed intervals. This design ensures that the reconstruction objective remains well-defined as the model progressively aggregates information across increasing temporal scales.

Hybrid Self-supervised Learning The Micro-Encoder is

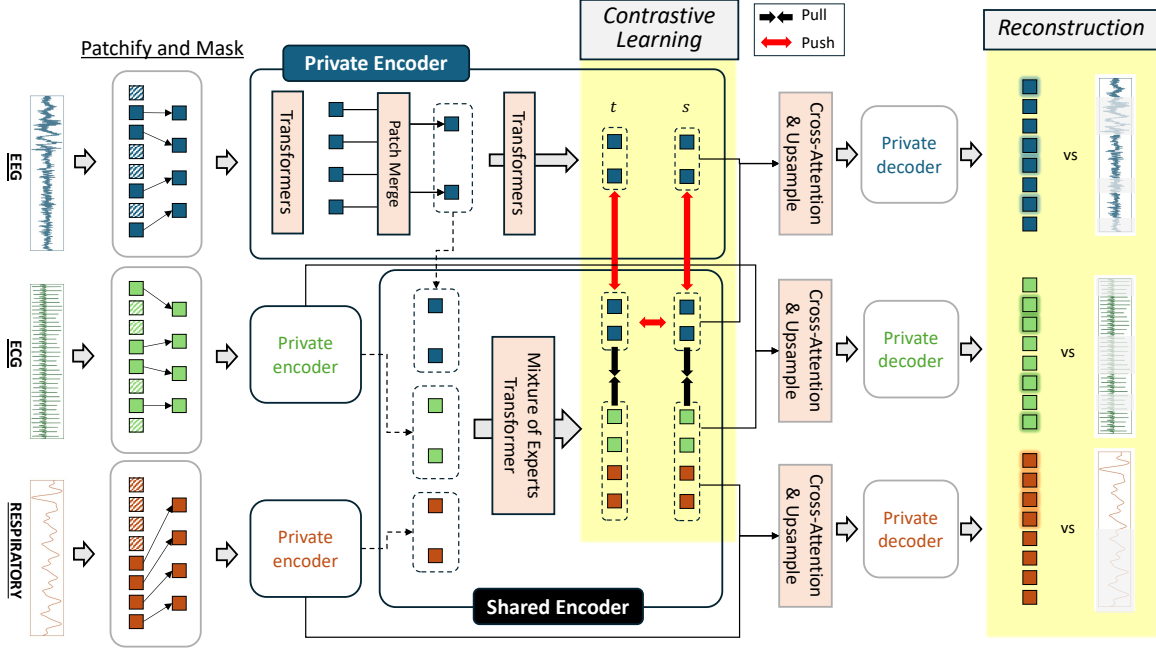


Figure 2. Micro-Encoder design and pretraining method. The Micro-Encoder adopts a private–shared encoder architecture, incorporating patch merging to improve computational efficiency in the shared encoder. The model is trained with a hybrid objective that combines masked autoencoding (reconstruction) and multi-modal contrastive learning to capture sleep micro-structure. For clarity and space constraints, only three representative modalities are shown.

optimized using a synergistic combination of two self-supervised paradigms: Masked Autoencoder (MAE) (He et al., 2022) and Contrastive Learning (Oord et al., 2018; Chen et al., 2020). Following the MAE framework, a fixed percentage of patches across all modalities is masked. To account for varying dominant frequencies of biosignals included in PSG, we use two different masking patterns. For high-frequency biosignals (EEG, EOG, EMG and ECG), we randomly mask a single patch (equivalent to 500ms), and for lower-frequency biosignals (respiratory and oxygen saturation), we randomly mask four consecutive patches (equivalent to 2 seconds). The encoders process only the visible patches. The latent features are then passed to a decoder to reconstruct the masked portion. By minimizing the reconstruction error of the raw signal on masked area, the model learns the fundamental *micro-structure* and local textures of the biosignals.

The reconstruction loss for modality i ($\mathcal{L}_{Mi,(i)}^{recon}$) is formally defined as follows:

$$\mathcal{L}_{Mi,(i)}^{recon} = \text{MSE}(m_i \cdot x_i, m_i \cdot \hat{x}_i) \quad (1)$$

where x_i and \hat{x}_i are the vectors representing original values and the predicted values of modality i , and m_i is a mask vector where masked patch area are marked as 1 and 0 otherwise. The loss is averaged over all modalities.

To further refine the latent space, we apply a CL loss to the shared encoder’s embeddings. This ensures that the shared representations are both temporally consistent and modality-agnostic. We define positive pairs as the average of shared

embeddings from different modalities sampled within the same timeslot, following the previous works (Thapa et al., 2024; 2026). This encourages the encoder to project different signals representing the same physiological state into a proximal region of the latent space. Two different kinds of negative pairs are used: temporal negatives and representation negatives. Temporal negative pairs consist of shared embeddings of the same modality from different timeslots. Representation negatives pairs consist of a shared embedding and a private embedding from the same signal. This specific negative pairing is crucial for feature disentanglement, ensuring the shared encoder does not inadvertently capture modality-specific noise.

The CL loss (\mathcal{L}_{Mi}^{CL}) is formally defined as follows:

$$\mathcal{L}_{Mi,(i,j),t}^{CL} = -\log \frac{\exp(\langle z_i^t, \bar{z}_{\neq i}^t \rangle / \tau)}{\sum_{s=1}^N \exp(\langle z_i^t, \bar{z}_{\neq i}^s \rangle / \tau) + \exp(\langle z_i^t, \tilde{z}_i^t \rangle / \tau)} \quad (2)$$

where z_i^t is the shared embeddings of modality i at timeslot t and $\bar{z}_{\neq i}^t$ is the average of shared embeddings from all modalities excluding i at t . \tilde{z}_i^t is the private embedding of modality i at t , N is the total number of timeslots in a batch and τ is a temperature scaling parameter. KoLeo regularization (Sablayrolles et al., 2018) (\mathcal{L}_{Mi}^{KoLeo}) is used together for better representation learning.

Final loss is calculated as the sum of reconstruction, contrastive and KoLeo loss as follows.:

$$\mathcal{L}_{Mi} = \mathcal{L}_{Mi}^{recon} + \lambda_{CL} \mathcal{L}_{Mi}^{CL} + \lambda_{KoLeo} \mathcal{L}_{Mi}^{KoLeo} \quad (3)$$

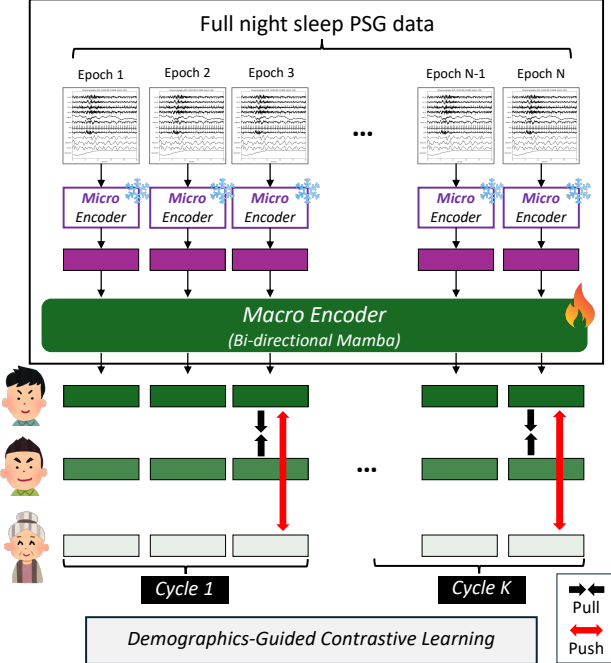


Figure 3. Macro-Encoder design and pretraining method. We utilize bi-directional Mamba layers for efficient long-sequence modeling. Demographic-Guided Contrastive Learning aligns the sleep macro-structure between subjects with objective metadata.

3.2. Macro-Encoder

The Macro-Encoder is designed to contextualize the local epoch-level embeddings within the broader *macro-structure* of a full night’s sleep. While the Micro-Encoder captures short-term physiological states, the Macro-Encoder models the temporal evolution of sleep patterns across the entire recording.

Macro-Encoder architecture As shown in Figure 3, the Macro-Encoder receives the complete sequence of epoch-by-epoch embeddings generated by the pretrained Micro-Encoder. To process these long-range dependencies, we employ Mamba layers (Gu & Dao, 2024). We specifically choose the Mamba architecture (a Selective State Space Model) over traditional Transformers due to its superior scaling properties and memory efficiency. Given that a standard full-night recording typically exceeds 800 epochs and large batch size expedites for effective contrastive learning used for training, Mamba’s linear scaling allows it to capture global context without the quadratic memory overhead associated with self-attention. Furthermore, we implement these layers in a bi-directional manner to address the inherent variability in recording durations across subjects, making fixed-length temporal alignment difficult especially at later stages. Bi-directionality allows the model to learn the macro-structure both from the sleep onset and from the sleep termination.

Demographic-guided Contrastive Learning (DGCL) To optimize the Macro-Encoder, we introduce a variant of contrastive learning that leverages demographic metadata, specifically age, sex and BMI as supervisory signals. These factors are primary determinants of sleep architecture, influencing parameters such as Slow Wave Sleep (SWS) or REM sleep duration and sleep fragmentation (Mander et al., 2017). Figure 4 shows the sleep stage distribution trend over full night, separated by age (Younger (18-60 yrs) and Older (> 60 yrs)), BMI (Non-obese and Obese) and sex, derived from a combined subset of our pretraining data (SHHS1/2, KISS and KVSS). The distributions reveal clear distinction between different groups. For example, the N3 proportion in the older, obese male group (bottom left) is significantly lower than that of younger, non-obese female group (top right) during the early stages of sleep. In addition, REM proportion in the later stages of the night vary considerably across different groups. These demographic attributes provide objective, noise-free ground truth, circumventing inter-scorer variability (Danker-Hopfe et al., 2004; 2009) and evolving clinical guidelines (Berry, 2012; Berry et al., 2017) associated with manual PSG labeling. Furthermore, the near-universal availability of demographic data ensures the scalability of this training strategy.

To effectively capture sleep cycles, we partition the full-night sequence into 90-minute intervals (180 epochs), corresponding to the average duration of a human ultradian sleep cycle (Dement & Kleitman, 1957). We then apply a soft-target contrastive objective that calculates the similarity between patient intervals based on their demographic profiles. Instead of traditional binary positive/negative pairs, we adopt a weighted similarity approach, inspired by generalized InfoNCE loss (Yang et al., 2023). For a given interval c and subject pair (i, j) , the loss for forward Mamba pass is formulated as follows:

$$\mathcal{L}_{Ma,(i,j),c} = -w_{i,j} \log \frac{\exp(\langle \vec{Z}_i^c, \vec{Z}_j^c \rangle / \rho)}{\sum_{k=1}^K \exp(\langle \vec{Z}_i^c, \vec{Z}_k^c \rangle / \rho)} \quad (4)$$

$$w_{i,j} = \frac{\exp(-d_{i,j}/v)}{\sum_{k=1}^K \exp(-d_{i,k}/v)}$$

where \vec{Z}_i^c and \vec{Z}_j^c are the refined latent features of the subjects i and j at the end of c -th interval in the forward pass, ρ and v are temperature scaling parameters and K is the total number of subjects in a batch. The *demographic distanced* $_{i,j}$ serves as the supervisory signal, calculated as a function of the mean absolute difference of age and BMI, with a penalty for sex mismatch:

$$d_{i,j} = (|\text{age}_i - \text{age}_j| + |\text{BMI}_i - \text{BMI}_j|)/2 + \lambda_{\text{sex}} \quad (5)$$

Here, age and BMI are z-score normalized and λ_{sex} is a constant penalty applied only when subjects i and j are

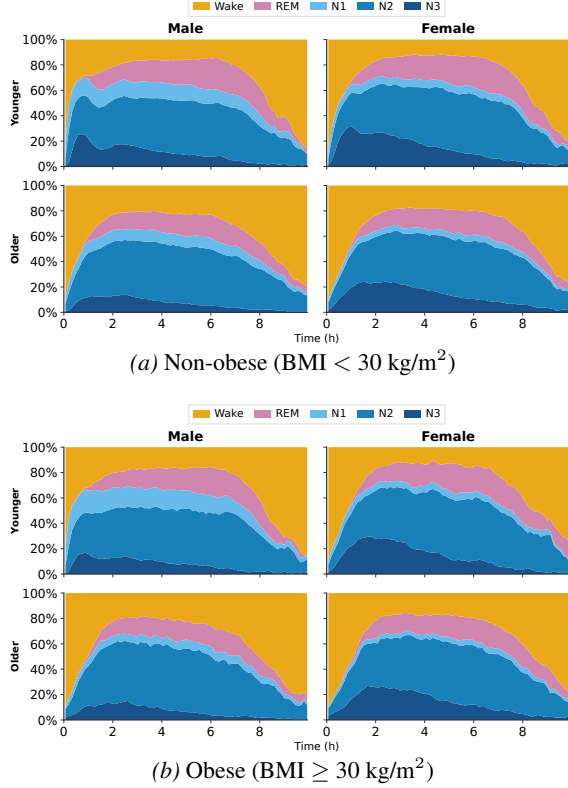


Figure 4. Sleep macro-structure variations across demographic groups. Sleep stage distributions over full-night recordings by sex, age (Younger: < 60 yrs; Older: ≥ 60 yrs) and BMI. N3 proportion in the early sleep period or REM sleep proportion in later stage varies significantly across groups. These demographic dependent patterns motivate our Demographic-Guided Contrastive Learning objective.

of different sex. The backward loss ($\overleftarrow{\mathcal{L}}_{Ma,(i,j),c}$) is defined symmetrically for the backward Mamba pass. The total Macro loss (\mathcal{L}_{Ma}) is aggregated over all intervals and subject pairs:

$$\mathcal{L}_{Ma} = \sum_c \sum_{i \neq j} \left(\overrightarrow{\mathcal{L}}_{Ma,(i,j),c} + \overleftarrow{\mathcal{L}}_{Ma,(i,j),c} \right) \quad (6)$$

This strategy effectively regularizes the latent space by pulling subjects with similar demographic profiles closer together while pushing disparate subjects further apart. To ensure stable convergence, we employ a stratified batch sampling strategy, maintaining balanced demographic distributions and similar sequence lengths within each batch.

3.3. Pretraining datasets and preprocessing

To pretrain *SleepMaMi*, we utilize the combination of open-sourced sleep datasets: the Sleep Heart Health Study (SHHS1/2) (Zhang et al., 2018; Quan et al., 1997), Korea Image-based Sleep Study (KISS) (Jeong et al., 2023), Korea Video Sleep Study (KVSS) (Jang et al., 2025), Physionet 2018 (PHY) (Goldberger et al., 2000; Ghas-

semi et al., 2018), Multi-Ethnic Study of Atherosclerosis (MESA) (Chen et al., 2015) and Osteoporotic Fractures in Men Study (MrOS) (Blackwell et al., 2011). The training split of SHHS1 and KISS are used for pretraining, with the partitioning scheme following the established protocols (Phan et al., 2021; Park et al., 2025). In total, we use 20,964 PSG recordings (158,028 hours) for pretraining.

All raw biosignals are resampled at 100 Hz to standardize the varying sampling rates across the diverse datasets. We applied a 0.3–40 Hz bandpass filter to the EEG and EOG signals, a 0.3–60 Hz bandpass filter to the ECG, and a 10 Hz highpass filter to the EMG. Additionally, a 60 Hz notch filter was applied to the EEG, EOG, ECG, and EMG signals to remove power-line interference. Respiratory signals were processed with a 15 Hz lowpass filter. Finally, all signals were z-score normalized prior to model input.

3.4. Implementation

The code is written in PyTorch and PyTorch Lightning wrapper. Both Macro- and Micro-Encoders are trained with AdamW (Loshchilov & Hutter, 2019) optimizer with cosine annealing (Loshchilov & Hutter, 2017) learning rate schedule. The training is done on $2 \times$ NVIDIA H100 HBM3 (VRAM 80GB) GPUs and the end-to-end pretraining takes approximately 10 hours. Flash attention-2 (Dao, 2023) is utilized in Transformer blocks for efficiency. More training details are provided in Appendix C.

4. Experiments and Results

4.1. Downstream Tasks

We evaluate *SleepMaMi* on downstream tasks including sleep stage classification, sleep disordered breathing (SDB) segmentation and disease prediction. To compare the performance of *SleepMaMi* to other contemporary foundation models we choose two time series foundation models (MOMENT (Goswami et al., 2024) and UniTS (Gao et al., 2024)) and a sleep foundation models (SleepFM-Disease (Thapa et al., 2026)) as baselines. Unless the baseline model’s input format requires specific settings (e.g. Sampling rate of 256 Hz for SleepFM-Disease), we use the same input with identical preprocessing.

4.1.1. SLEEP STAGE CLASSIFICATION

Sleep staging refers to classifying each 30-second epoch into one of five sleep stages: Wake, Rapid Eye Movement (REM), Non-REM stages N1, N2 and N3. We conduct linear probing (Alain & Bengio, 2017) on target datasets to objectively test the quality of the learned representations. Weighted cross entropy loss is used to account for imbalanced sleep stage distribution. In addition, following conventional sleep scoring protocols, we truncated continuous

Table 1. Sleep stage classification results. The results demonstrate the effectiveness of *SleepMaMi* compared to time series and sleep foundation models. The evaluation is done on the test split of SHHS1 and KISS datasets

Dataset	Category	Models	Accuracy	Macro-F1	Kappa
SHHS1	Time series	MOMENT-Base	79.4	65.6	70.0
	Foundation model	UniTS	64.2	59.2	53.3
	Sleep	SleepFM-Disease	69.7	56.3	55.9
	Foundation model	<i>SleepMaMi</i> (Ours)	81.9	74.1	70.0
KISS	Time series	MOMENT-Base	69.8	66.3	59.7
	Foundation model	UniTS	60.3	58.8	49.8
	Sleep	SleepFM-Disease	57.6	58.4	46.1
	Foundation model	<i>SleepMaMi</i> (Ours)	62.8	60.6	51.2

Table 2. SDB segmentation results. The results demonstrate *SleepMaMi*’s superior capability to capture fine-grained details, compared to time series and sleep foundation models. The evaluation is done on the test split of SHHS1 and KISS datasets. Macro-F1 is emphasized as a more robust metric under severe class imbalance in SDB labels.

Dataset	Category	Models	Accuracy	Macro-F1
SHHS1	Time series	MOMENT-Base	73.4	33.4
	Foundation model	UniTS	88.2	48.8
	Sleep	SleepFM-Disease	77.5	39.4
	Foundation model	<i>SleepMaMi</i> (Ours)	77.3	60.6
KISS	Time series	MOMENT-Base	76.0	58.5
	Foundation model	UniTS	79.8	63.6
	Sleep	SleepFM-Disease	79.6	65.1
	Foundation model	<i>SleepMaMi</i> (Ours)	81.8	75.4

Wake epochs to 30 minutes before the first non-Wake epoch and 30 minutes after the last non-Wake epoch.

The sleep staging results are provided in Table 1. On SHHS1, *SleepMaMi* outperforms all baselines, demonstrating its superior capability in capturing sleep-specific physiological features. On KISS, however, MOMENT achieves higher performance. We hypothesize that this discrepancy stems from distribution shift across recording hardware. While the majority of our pretraining data was collected using Compumedics hardware, the KISS dataset was collected from Nox and Embla PSG systems (see Appendix. 7). This suggests that *SleepMaMi* may partially benefit from sensitivity to specific signal characteristics of Compumedics sensors, which could influence performance under hardware distribution shifts. These results highlight a trade-off between sleep-specific representation learning and sensor-agnostic generalization, suggesting that future work incorporating multi-hardware pretraining or explicit domain adaptation may further improve robustness across heterogeneous PSG systems.

4.1.2. SDB SEGMENTATION

SDB segmentation requires the high-resolution classification of each one-second interval into categories of normal breathing or disordered breathing (specifically hypopnea or apnea). Consistent with our evaluation protocol for sleep stage classification, we evaluate the learned representations

via a linear probing task optimized with weighted cross entropy loss.

The results are summarized in Table 2. It demonstrates that *SleepMaMi* significantly outperforms the established baselines, particularly in capturing the fine-grained physiological transitions necessary for precise segmentation. Although the raw accuracy on SHHS1 dataset appears slightly lower than some baselines, this metric is skewed by the severe class imbalance of SDB labels (10.6:1). In this context, the Macro-F1 score provides a more robust and equitable comparison. Notably, our model achieves a substantial performance gain over SleepFM. We attribute this superior performance to our Micro-Encoder’s hybrid pretraining strategy. While SleepFM relies solely on CL, which focuses on global signal alignment, our integration of MAE reconstruction encourages the model to learn the micro-structures of respiratory signals. This increased sensitivity to local signal fluctuations proves critical for the second-by-second detection of subtle breathing disruptions.

4.1.3. DISEASE PREDICTION

We utilize the SHHS dataset’s disease histories to perform PSG-based disease prediction. We also employ linear probing for this task using the Cox Proportional Hazard (Cox PH) loss (Cox, 1972; Katzman et al., 2018), defined by the following negative log-partial likelihood:

$$\mathcal{L}_{PH} = \frac{1}{N_e} \sum_{i=1}^N -\delta_i \left(h_i - \log \sum_{k \in R_i} \exp(h_k) \right) \quad (7)$$

where h_i represents the predicted risk score for subject i , and $\delta_i \in \{0, 1\}$ is a binary indicator denoting whether subject i experienced the event (disease occurrence). $N_e = \sum_i \delta_i$ is the total number of the events within the population of N subjects. The risk set R_i consists of all subjects whose time-to-event (or censoring) is greater than or equal to that of subject i . Following the evaluation protocol of SleepFM-Disease (Thapa et al., 2026), we assess the predictive performance of *SleepMaMi* across six diseases. Performance is quantified via Harrell’s concordance index (C-Index). The results are summarized in Table 3. *SleepMaMi* shows comparable performance to SleepFM-Disease, highlighting its potential for reliable clinical application in sleep-based healthcare.

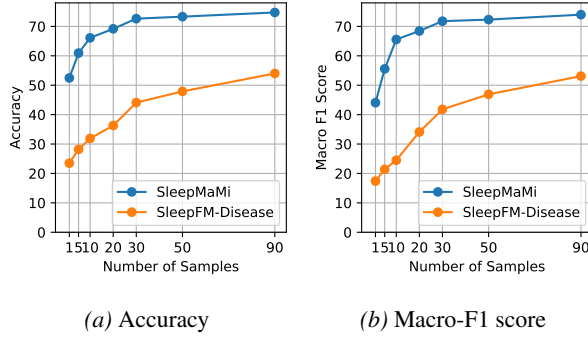
4.2. Few-shot Evaluation

To evaluate the fast adaptation ability of *SleepMaMi* to unseen data, we conduct a few-shot evaluation using the IS-RUC dataset (Khalighi et al., 2016). In this setup, Subgroup 1 is utilized for fine-tuning and validation, while Subgroups 2 and 3 were combined to form the test set. We restricted the fine-tuning data from Subgroup 1 to specific increments ($n = 1, 5, 10, 20, 30, 50, 90$) to measure sleep staging per-

Table 3. Disease prediction. C-Index is reported on 6 selected diseases from SHHS1 dataset. *SleepMaMi* shows comparable performance to the state-of-the-art PSG-based disease prediction model.

Models	Disease Outcomes					
	Angina	CVD death	CHF	CHD death	MI	Stroke
<i>C-Index</i>						
SleepFM-Disease	0.632	0.791	0.764	0.781	0.636	0.729
<i>SleepMaMi</i> (Ours)	0.778	0.788	0.793	0.776	0.662	0.718

*CVD death: CardioVascular Disease death, CHF: Congestive Heart Failure, CHD death: Coronary Heart Disease death, MI: Myocardial Infarctions



(a) Accuracy (b) Macro-F1 score

Figure 5. Few shot evaluation. Accuracy and Macro-F1 is measured with varying number of finetuning samples. *SleepMaMi* shows label-efficient adaptation to unseen dataset thanks to well-generalized embeddings derived from large-scale pretraining data.

formance on the test split. As illustrated in Figure 5, *SleepMaMi* demonstrates impressive label efficiency. With only a single training sample, the model achieves an accuracy of 52.5% and a F1 score of 44.1%. When the sample size increases to 30, the accuracy and F1 score rise to 72.6% and 71.8%, respectively—performing only 2.1% and 2.2% lower than the model trained on the entire dataset. These results validate the practicality of *SleepMaMi* as a robust foundation model to generalize well in data-constrained scenarios.

4.3. Contribution of the Macro-Encoder

Unlike existing models that focus exclusively on sleep micro-structure, *SleepMaMi* incorporates a Macro-Encoder to integrate high-level sleep *macro-structure* with micro-structure. To evaluate the added value of the Macro-Encoder, we conduct a comparative analysis using two classification and two regression tasks, evaluating embeddings from the Micro-Encoder alone against those from the full *SleepMaMi* architecture. As summarized in Table 4, the integration of the Macro-Encoder yielded performance gains across all four tasks. Notably, although only sex and age are implicitly encoded during pretraining, the Macro-Encoder significantly enhanced performance in sleep staging and AHI estimation. These results suggest that DGCL fosters a superior representation of the global sleep architecture, benefiting a

Table 4. Performance comparison between Micro-only and *SleepMaMi*. The integration of the Macro-Encoder consistently improves performance across all tasks, validating the effectiveness of DGCL in incorporating sleep macro-structure.

Models	Classification (Acc. \uparrow)		Regression (MAE \downarrow)	
	Sleep stage	Sex	Age	AHI
Micro-Encoder only	79.8	80.1	9.45	9.69
<i>SleepMaMi</i>	81.9	88.2	6.73	8.40

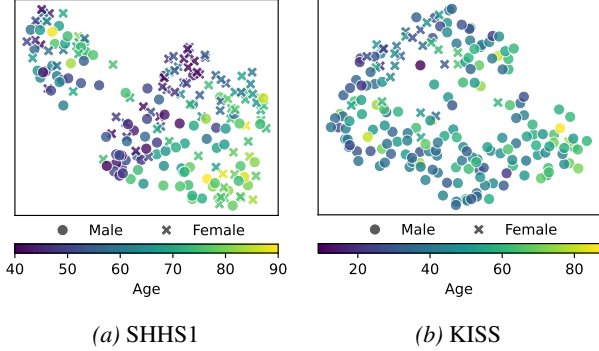


Figure 6. Macro-embeddings visualization. Per-subject latent embeddings from Macro-Encoder is visualized using U-MAP. Each point represents a single subject’s embeddings where color and symbol represents age and sex, respectively. More visualizations are available in Appendix. D.3

wide range of downstream sleep-related tasks.

4.4. Embedding Analysis and Visualization

To qualitatively assess how effectively the Macro-Encoder captures demographic features within the latent space, we visualize the subject-level embeddings using U-MAP, as shown in Figure 6. This analysis is performed on 200 subjects randomly sampled from the test splits of the SHHS1 and KISS datasets. The visualization reveals clear clustering based on demographic attributes, with subjects of similar age and sex residing closely within the embedding space. This distinct separation confirms that our DGCL framework successfully maps demographic characteristics into the latent space, providing the model with a grounded, subject-aware context for sleep analysis.

5. Conclusion

In this study, we introduce *SleepMaMi*, a novel sleep foundation model that integrates both sleep *micro-* and *macro-structure*, pretrained on 20,964 PSG recordings. Our architecture utilizes a dual-encoder design: a Micro-Encoder with a private-shared transformer backbone optimized via hybrid of MAE and CL to capture the fine-grained physiological features and a Mamba-based Macro-Encoder to model long-range temporal dependencies across full night. DGCL is employed to train the Macro-Encoder, which leverages objective metadata to encode sleep macro-structure into

the model. Extensive evaluations demonstrate that *SleepMaMi* outperforms existing foundation models across a wide spectrum of tasks. Furthermore, the model exhibits strong label-efficient adaptation, proving its utility as a robust and practical foundation for clinical sleep analysis even in data-constrained environment.

References

Ahn, H. K., Na, Y., and Shin, H.-W. Refining sleep-disordered breathing annotations across multiple public sleep study datasets. *Journal of Sleep Research*, pp. e70264, 2025.

AIHub. Aihub. image of sleep quality assessment and sleep disorder diagnosis. <https://www.aihub.or.kr/aihubdata/data/view.do?currMenu=&topMenu=&aihubDataSet=realm&dataSetSn=210>, 2020.

Alain, G. and Bengio, Y. Understanding intermediate layers using linear classifier probes. In *International Conference on Learning Representations (ICLR), Workshop Track*, 2017.

Benjafield, A. V., Ayas, N. T., Eastwood, P. R., Heinzer, R., Ip, M. S., Morrell, M. J., Nunez, C. M., Patel, S. R., Penzel, T., Pépin, J.-L., et al. Estimation of the global prevalence and burden of obstructive sleep apnoea: a literature-based analysis. *The Lancet respiratory medicine*, 7(8): 687–698, 2019.

Berry, R. The aasm manual for the scoring of sleep and associated events. *Rules, Terminology and Technical Specifications. Version 2*, 2, 2012.

Berry, R. B., Brooks, R., Gamaldo, C., Harding, S. M., Lloyd, R. M., Quan, S. F., Troester, M. T., and Vaughn, B. V. Aasm scoring manual updates for 2017 (version 2.4), 2017.

Blackwell, T., Yaffe, K., Ancoli-Israel, S., Redline, S., Ensrud, K. E., Stefanick, M. L., Laffan, A., Stone, K. L., and in Men Study Group, O. F. Associations between sleep architecture and sleep-disordered breathing and cognition in older community-dwelling men: the osteoporotic fractures in men sleep study. *Journal of the American Geriatrics Society*, 59(12):2217–2225, 2011.

Brink-Kjaer, A., Leary, E. B., Sun, H., Westover, M. B., Stone, K. L., Peppard, P. E., Lane, N. E., Cawthon, P. M., Redline, S., Jenum, P., et al. Age estimation from sleep studies using deep learning predicts life expectancy. *NPJ digital medicine*, 5(1):103, 2022.

Chen, T., Kornblith, S., Norouzi, M., and Hinton, G. A simple framework for contrastive learning of visual representations. In *International conference on machine learning*, pp. 1597–1607. PmLR, 2020.

Chen, X., Wang, R., Zee, P., Lutsey, P. L., Javaheri, S., Alcántara, C., Jackson, C. L., Williams, M. A., and Redline, S. Racial/ethnic differences in sleep disturbances: the multi-ethnic study of atherosclerosis (mesa). *Sleep*, 38(6):877–888, 2015.

Choi, Y. R., Eo, G., Yoon, W., Lee, H., Jang, H., Kim, D. Y., Shin, H.-W., and Kim, H.-S. Poster: Home-based, on-device non-invasive obstructive sleep apnea monitoring with infrared video. In *Proceedings of the 22nd Annual International Conference on Mobile Systems, Applications and Services*, pp. 708–709, 2024.

Cox, D. R. Regression models and life-tables. *Journal of the Royal Statistical Society: Series B (Methodological)*, 34(2):187–202, 1972.

Danker-Hopfe, H., Kunz, D., Gruber, G., Klösch, G., Lorenzo, J. L., Himanen, S.-L., Kemp, B., Penzel, T., Röschke, J., Dorn, H., et al. Interrater reliability between scorers from eight european sleep laboratories in subjects with different sleep disorders. *Journal of Sleep Research*, 13(1):63–69, 2004.

Danker-Hopfe, H., Anderer, P., Zeitlhofer, J., Boeck, M., Dorn, H., Gruber, G., Heller, E., Loretz, E., Moser, D., Parapatics, S., et al. Interrater reliability for sleep scoring according to the rechtschaffen & kales and the new aasm standard. *Journal of Sleep Research*, 18(1):74–84, 2009.

Dao, T. Flashattention-2: Faster attention with better parallelism and work partitioning. *arXiv preprint arXiv:2307.08691*, 2023.

Das, A., Kong, W., Sen, R., and Zhou, Y. A decoder-only foundation model for time-series forecasting. In *Forty-first International Conference on Machine Learning*, pp. 10148–10167, 2024.

Dement, W. and Kleitman, N. Cyclic variations in eeg during sleep and their relation to eye movements, body motility, and dreaming. *Electroencephalography and Clinical Neurophysiology*, 9(4):673–690, 1957.

Gao, S., Koker, T., Queen, O., Hartvigsen, T., Tsilgkaridis, T., and Zitnik, M. Units: A unified multi-task time series model. *Advances in Neural Information Processing Systems*, 37:140589–140631, 2024.

Ghassemi, M. M., Moody, B. E., Lehman, L.-W. H., Song, C., Li, Q., Sun, H., Mark, R. G., Westover, M. B., and Clifford, G. D. You snooze, you win: the physionet/computing in cardiology challenge 2018. In *2018 Computing in Cardiology Conference*, volume 45, pp. 1–4. IEEE, 2018.

Goldberger, A. L., Amaral, L. A., Glass, L., Hausdorff, J. M., Ivanov, P. C., Mark, R. G., Mietus, J. E., Moody, G. B., Peng, C.-K., and Stanley, H. E. Physiobank, physiotoolkit, and physionet: components of a new research resource for complex physiologic signals. *Circulation*, 101(23):e215–e220, 2000.

Goswami, M., Szafer, K., Choudhry, A., Cai, Y., Li, S., and Dubrawski, A. Moment: A family of open time-series foundation models. In *International Conference on Machine Learning*, pp. 16115–16152, 2024.

Gu, A. and Dao, T. Mamba: Linear-time sequence modeling with selective state spaces. In *First conference on language modeling*, 2024.

Guillot, A., Sauvet, F., During, E. H., and Thorey, V. Dreem open datasets: Multi-scored sleep datasets to compare human and automated sleep staging. *IEEE Transactions on Neural Systems and Rehabilitation Engineering*, 28(9):1955–1965, 2020.

He, K., Chen, X., Xie, S., Li, Y., Dollár, P., and Girshick, R. Masked autoencoders are scalable vision learners. In *Proceedings of the IEEE/CVF conference on computer vision and pattern recognition*, pp. 16000–16009, 2022.

Jang, K., Choi, Y. R., Park, D., Shin, H.-W., and Kim, H.-S. *Poster: Home-based, On-Device, Non-contact Sleep Staging with Infrared Video*, pp. 1380–1382. Association for Computing Machinery, New York, NY, USA, 2025. ISBN 9798400711299. URL <https://doi.org/10.1145/3680207.3765693>.

Jeong, J., Yoon, W., Lee, J.-G., Kim, D., Woo, Y., Kim, D.-K., and Shin, H.-W. Standardized image-based polysomnography database and deep learning algorithm for sleep-stage classification. *Sleep*, 46(12):zsad242, 2023.

Katzman, J. L., Shaham, U., Cloninger, A., Bates, J., Jiang, T., and Kluger, Y. DeepSurv: Personalized treatment recommender system using a Cox proportional hazards deep neural network. *BMC Medical Research Methodology*, 18(1):1–12, 2018.

Khalighi, S., Sousa, T., Santos, J. M., and Nunes, U. Isruc-sleep: A comprehensive public dataset for sleep researchers. *Computer methods and programs in biomedicine*, 124:180–192, 2016.

Lee, S., Yu, Y., Back, S., Seo, H., and Lee, K. Sleepyco: Automatic sleep scoring with feature pyramid and contrastive learning. *Expert Systems with Applications*, 240:122551, 2024.

Lepikhin, D., Lee, H., Xu, Y., Chen, D., Firat, O., Huang, Y., Krikun, M., Shazeer, N., and Chen, Z. Gshard: Scaling giant models with conditional computation and automatic sharding. *arXiv preprint arXiv:2006.16668*, 2020.

Levy, J., Álvarez, D., Del Campo, F., and Behar, J. A. Deep learning for obstructive sleep apnea diagnosis based on single channel oximetry. *Nature Communications*, 14(1):4881, 2023.

Loshchilov, I. and Hutter, F. SGDR: Stochastic gradient descent with warm restarts. In *International Conference on Learning Representations*, 2017. URL <https://openreview.net/forum?id=Skq89Scxx>.

Loshchilov, I. and Hutter, F. Decoupled weight decay regularization. In *International Conference on Learning Representations*, 2019. URL <https://openreview.net/forum?id=Bkg6RiCqY7>.

Mander, B. A., Winer, J. R., and Walker, M. P. Sleep and human aging. *Neuron*, 94(1):19–36, 2017.

Oord, A. v. d., Li, Y., and Vinyals, O. Representation learning with contrastive predictive coding. *arXiv preprint arXiv:1807.03748*, 2018.

Park, K., Hong, J., Lee, W., Shin, H.-W., and Kim, H.-S. Distillsleep: real-time, on-device, interpretable sleep staging from single-channel electroencephalogram. *SLEEPJ*, 48(12):zsaf240, 2025.

Perslev, M., Darkner, S., Kempfner, L., Nikolic, M., Jenum, P. J., and Igel, C. U-sleep: resilient high-frequency sleep staging. *NPJ Digital Medicine*, 4(1):72, 2021.

Phan, H., Andreotti, F., Cooray, N., Chén, O. Y., and De Vos, M. Seqsleepnet: end-to-end hierarchical recurrent neural network for sequence-to-sequence automatic sleep staging. *IEEE Transactions on Neural Systems and Rehabilitation Engineering*, 27(3):400–410, 2019.

Phan, H., Chén, O. Y., Tran, M. C., Koch, P., Mertins, A., and De Vos, M. Xsleepnet: Multi-view sequential model for automatic sleep staging. *IEEE Transactions on Pattern Analysis and Machine Intelligence*, 44(9):5903–5915, 2021.

Phan, H., Mikkelsen, K., Chén, O. Y., Koch, P., Mertins, A., and De Vos, M. Sleeptransformer: Automatic sleep staging with interpretability and uncertainty quantification. *IEEE Transactions on Biomedical Engineering*, 69(8):2456–2467, 2022.

Quan, S. F., Howard, B. V., Iber, C., Kiley, J. P., Nieto, F. J., O’Connor, G. T., Rapoport, D. M., Redline, S., Robbins, J., Samet, J. M., et al. The sleep heart health study: design, rationale, and methods. *Sleep*, 20(12):1077–1085, 1997.

Retamales, G., Gavidia, M. E., Bausch, B., Montanari, A. N., Husch, A., and Goncalves, J. Towards automatic home-based sleep apnea estimation using deep learning. *npj Digital Medicine*, 7(1):144, 2024.

Sablayrolles, A., Douze, M., Schmid, C., and Jégou, H. Spreading vectors for similarity search. *arXiv preprint arXiv:1806.03198*, 2018.

Shazeer, N. Glu variants improve transformer. *arXiv preprint arXiv:2002.05202*, 2020.

Su, J., Ahmed, M., Lu, Y., Pan, S., Bo, W., and Liu, Y. Roformer: Enhanced transformer with rotary position embedding. *Neurocomputing*, 568:127063, 2024.

Sun, H., Paixao, L., Oliva, J. T., Goparaju, B., Carvalho, D. Z., van Leeuwen, K. G., Akeju, O., Thomas, R. J., Cash, S. S., Bianchi, M. T., et al. Brain age from the electroencephalogram of sleep. *Neurobiology of aging*, 74:112–120, 2019.

Supratak, A., Dong, H., Wu, C., and Guo, Y. Deepsleepnet: A model for automatic sleep stage scoring based on raw single-channel eeg. *IEEE Transactions on Neural Systems and Rehabilitation Engineering*, 25(11):1998–2008, 2017.

Thapa, R., He, B., Kjaer, M. R., Moore, H., Ganjoo, G., Mignot, E., and Zou, J. Sleepfm: Multi-modal representation learning for sleep across brain activity, ecg and respiratory signals. *arXiv preprint arXiv:2405.17766*, 2024.

Thapa, R., Kjaer, M. R., He, B., Covert, I., Moore IV, H., Hanif, U., Ganjoo, G., Westover, M. B., Jenum, P., Brink-Kjaer, A., et al. A multimodal sleep foundation model for disease prediction. *Nature Medicine*, pp. 1–11, 2026.

Vaswani, A., Shazeer, N., Parmar, N., Uszkoreit, J., Jones, L., Gomez, A. N., Kaiser, Ł., and Polosukhin, I. Attention is all you need. In *Advances in Neural Information Processing Systems*, volume 30, 2017.

Woo, G., Liu, C., Kumar, A., Xiong, C., Savarese, S., and Sahoo, D. Unified training of universal time series forecasting transformers. In *Proceedings of the 41st International Conference on Machine Learning*, volume 235, pp. 53140–53164. PMLR, 2024.

Xiong, R., Yang, Y., He, D., Zheng, K., Zheng, S., Xing, C., Zhang, H., Lan, Y., Wang, L., and Liu, T. On layer normalization in the transformer architecture. In *International conference on machine learning*, pp. 10524–10533. PMLR, 2020.

Yang, Y., Liu, X., Wu, J., Borac, S., Katabi, D., Poh, M.-Z., and McDuff, D. Simper: Simple self-supervised learning of periodic targets. In *International Conference on Learning Representations*, 2023. URL <https://openreview.net/forum?id=EKpMeEV0hOo>.

Zhang, B. and Sennrich, R. Root mean square layer normalization. *Advances in neural information processing systems*, 32, 2019.

Zhang, G.-Q., Cui, L., Mueller, R., Tao, S., Kim, M., Rueschman, M., Mariani, S., Mobley, D., and Redline, S. The national sleep research resource: towards a sleep data commons. *Journal of the American Medical Informatics Association*, 25(10):1351–1358, 2018.

A. Datasets

The brief description of the datasets used for this research is provided below. Table 5 provides the summary statistics extracted from each dataset used for pretraining. Table 6 provides the summary statistics from the data not used for pretraining, but used for downstream tasks. Table 7 lists the channels included in each modality from different datasets.

A.1. Physionet 2018 (PHY) Dataset

The PhysioNet 2018 dataset, originally curated for the 2018 PhysioNet/CinC Challenge (Goldberger et al., 2000; Ghassemi et al., 2018), was provided by the Computational Clinical Neurophysiology Laboratory and the Clinical Data Animation Laboratory at Massachusetts General Hospital. Although the challenge primarily focused on arousal detection, the dataset includes expert-labeled sleep stages for 994 subjects. An additional 991 recordings were reserved for testing purposes; however, their labels remain private. In this study, we utilized both the labeled training set and the unlabeled test set for pretraining *SleepMaMi*. All signals were sampled at 200 Hz, with sleep stages scored according to the American Academy of Sleep Medicine (AASM) guidelines.

A.2. Sleep Heart Health Study (SHHS) Dataset

The Sleep Heart Health Study (SHHS) (Zhang et al., 2018; Quan et al., 1997) is a multicenter cohort initiative organized by the National Heart, Lung, and Blood Institute. This study consists of data collected over two visits. SHHS1 was collected from the initial visit, conducted between 1995 and 1998, which involved 6,441 men and women aged 40 and older. SHHS2 was collected from the second visit, conducted between 2001 and 2003, which involved 3,295 participants. Polysomnography (PSG) was recorded in-home by trained technicians and included various physiological signals: EEG (C3-A2, C4-A1), dual-channel EOG, EMG, respiratory effort, airflow, oxygen saturation, ECG, and body position. In alignment with the experimental protocol of XSleepNet (Phan et al., 2021), we partitioned the dataset by reserving 30% for testing. From the remaining 70%, 100 subjects were set aside for validation, with the balance used for model training. The train split of SHHS1 is used for pretraining and finetuning for downstream tasks. The entire SHHS2 dataset is used for pretraining and not used for downstream tasks.

A.3. Korea Image-based Sleep Study (KISS) Dataset

The Korea Image-based Sleep Study (KISS) dataset (Jeong et al., 2023) is a standardized, image-based polysomnography (PSG) repository. Collected between 2013 and 2020 across four sleep centers, the dataset utilizes recordings from Embla and NOX-A1 PSG systems, totaling 10,253 records. Expert scoring was conducted in accordance with AASM version 2.6 guidelines (Berry, 2012; Berry et al., 2017). Each record captures 21 distinct biosignals including various EEG, EOG, and EMG channels alongside respiratory and movement data. The data is publicly accessible via AI Hub (AIHub, 2020). Following the experimental setup by Jeong *et al.* (Jeong et al., 2023), we selected 7,579 records and implemented an 80%/20% split for training and validation/test on a patient-wise basis. The train split of KISS is used for pretraining and finetuning for downstream tasks.

Table 5. The dataset statistics used for pretraining. Missing values result from study design or anonymized data.

Dataset	Records	Subjects	Age (years)	BMI	Sex % (Female/Male)	Stage count						Stage ratio (%)				
						W	N1	N2	N3	REM	Total	W	N1	N2	N3	REM
PHY-Train	993	993	55.2 ± 14.3	N/A	33 / 67	145,558	135,409	372,208	101,678	113,859	868,712	17	16	42	12	13
PHY-Test	989	989	54.8 ± 14.3	N/A	37 / 63											N/A
SHHS1	3,667	3,667	63.1 ± 11.5	28.2 ± 5.2	52 / 48	739,301	136,407	1,519,573	472,529	516,768	3,384,578	22	4	45	14	15
SHHS2	2,554	2,554	67.6 ± 10.4	28.3 ± 5.0	54 / 46	683,291	106,964	1,103,742	303,068	395,437	2,592,502	26	4	43	12	15
KISS	6,064	6,064	44.8 ± 14.5	25.8 ± 4.3	20 / 80	981,362	665,497	1,556,469	601,227	660,186	4,464,741	22	15	35	13	15
KVSS	881	881	51.4 ± 14.2	26.8 ± 4.4	24 / 76	143,041	129,225	271,190	47,538	97,667	688,661	21	19	39	7	14
MrOS1	2,768	2,768	76.4 ± 5.5	27.1 ± 3.8	0 / 100	945,515	129,239	1,236,682	221,334	381,577	2,914,347	32	4	43	8	13
MrOS2	994	994	81.0 ± 4.4	26.9 ± 3.8	0 / 100	382,152	80,312	425,515	45,040	129,942	1,062,961	36	8	40	4	12
MESA	2,054	2,054	69.4 ± 9.1	28.7 ± 5.5	54 / 46	598,750	203,837	854,634	149,770	268,646	2,075,637	29	10	41	7	13

Table 6. The dataset statistics used for downstream evaluation.

Dataset	Records	Subjects	Age (years)	BMI	Sex % (Female/Male)	Stage count						Stage ratio (%)					
						W	N1	N2	N3	REM	Total	W	N1	N2	N3	REM	
SHHS1-Val	99	99	62.0 ± 11.7	27.8 ± 4.2	54 / 46	20,178	3,544	40,377	11,831	13,740	89,670	23	4	45	13	15	
SHHS1-Test	1,617	1,617	63.4 ± 11.5	28.0 ± 5.0	53 / 47	323,871	61,191	671,916	203,864	226,113	1,486,955	22	4	45	14	15	
KISS-Val	748	748	44.7 ± 14.1	26.0 ± 4.3	22 / 78	121,319	87,032	187,347	71,362	78,128	545,188	22	16	34	13	14	
KISS-Test	767	767	45.4 ± 14.3	26.0 ± 4.1	16 / 84	125,315	83,396	198,155	73,154	83,428	563,448	22	15	35	13	15	
ISRUC-SG1	100	100	51.1 ± 15.9	N/A	44 / 56	20,979	11,513	28,287	17,480	11,928	90,187	23	13	31	19	13	
ISRUC-SG2	16	8	46.9 ± 17.5	N/A	25 / 75	2,282	2,211	5,042	2,609	2,063	14,207	16	16	35	18	15	
ISRUC-SG3	10	10	39.6 ± 9.6	N/A	10 / 90	1,817	1,248	2,678	2,035	1,111	8,889	20	14	30	23	12	

Table 7. Channels and sampling rates included in different modalities across datasets. The manufacturer of PSG recording machine is also provided. When sampling rates are same across different channels in the modality, we only write once at the top row.

Modality	KISS / KVSS		SHHS1		SHHS2		PHY		MESA		MrOS1 / 2	
	Ch.	SR (Hz)	Ch.	SR (Hz)								
EEG	C3-M2	200	C3-A2	125	C3-A2	125	C3-M2	200	C4-M1	256	C3-M2	256
	C4-M1		C4-A1		C4-A1		C4-M1		Oz-Cz		C4-M1	
	O1-M2						O1-M2		Fz-Cz		O1-M2	
	O2-M1						O2-M1				O2-M1	
EOG	E1-M2	200	EOG (L)	125	EOG (L)	125	E1-M2	200	EOG (L)	256	EOG (L)	256
EMG	Chin EMG	200	EMG	125	EMG	125	Chin1-Chin2	200	Chin EMG	256	EMG (L)-EMG (R)	256
ECG	ECG	200	ECG	125	ECG	125	ECG	250	ECG	256	ECG1-ECG2	512
Respiratory	Flow	200	Flow	10	Flow	10	Flow	200	Flow	32	Flow	64
	Thermistor		Thorax		Thorax		Thorax		Thorax		Thermistor	16
	Thorax		Abdomen		Abdomen		Abdomen		Abdomen		Thorax	
Oxygen Sat.	Saturation	200	Oximetry	1	Oximetry	1	SaO2	200	SpO2	1	SpO2	1
Manufacturer	Nox, Embla		Compumedics		Compumedics		Unknown		Compumedics		Compumedics	

A.4. Korea Video Sleep Study (KVSS) Dataset

The Korea Video Sleep Study (KVSS) dataset is a retrospectively constructed, multi-center clinical cohort that provides synchronized infrared sleep video and polysomnography (PSG) with expert annotations (Choi et al., 2024). Data were collected under IRB-approved protocols from three hospitals (Chungnam National University Hospital, The Catholic University of Korea St. Vincent’s Hospital, and Hallym University Hospital). Across sites, 936 PSG examinations with synchronized infrared video were identified, and 881 PSG video pairs were included after screening and quality control. Recordings were obtained during routine clinical studies for various sleep-related indications, including suspected OSA, insomnia, PLMD, and RBD, with infrared videos recorded in parallel with PSG to ensure temporal alignment. Despite minor site-specific differences in camera placement and illumination, all videos were standardized to MP4 at 640×480 resolution and 5 fps. PSG was stored in European Data Format (EDF), and sleep stages (Wake, N1, N2, N3, REM) and AASM-defined events were annotated by certified technologists and reviewed by sleep physicians. The dataset underwent de-identification and expert cross-checking to verify synchronization and address obvious scoring inconsistencies. In this work, KVSS is used only as a PSG dataset, and we leverage the recorded PSG signals and associated subject metadata without using expert annotations or the infrared videos.

A.5. Multi-Ethnic Study of Atherosclerosis (MESA) Dataset

The Multi-Ethnic Study of Atherosclerosis (MESA) (Chen et al., 2015) is a multicenter cohort of 6,814 adults aged 45–84 years from four racial/ethnic groups (White, Black, Hispanic, and Chinese-American). As part of Exam 5 (2010–2013), the MESA Sleep exam enrolled 2,237 participants who completed single-night unattended in-home polysomnography (PSG) and wrist actigraphy. PSG was set up during an in-home evening visit by trained staff, and sleep staging and respiratory events were scored at a centralized sleep reading center using standardized procedures. The National Sleep Research Resource (NSRR) release provides PSG recordings in European Data Format (EDF) and XML annotation files for sleep

staging and respiratory event scoring. Respiratory event annotations were harmonized via rule-based post-processing of the original labels to ensure consistent criteria across datasets, and details are described in (Ahn et al., 2025). The PSG includes EEG (Fz-Cz, Cz-Oz, C4-A1), EOG, EMG, ECG, nasal airflow, thoracic and abdominal respiratory effort, oxygen saturation, and body position. In this work, we utilize the C4-A1 EEG. Recordings missing any required channel were excluded. 2,054 participants were included in the final analytic cohort.

A.6. Osteoporotic Fractures in Men Study (MrOS) Dataset

The Osteoporotic Fractures in Men Sleep Study (MrOS Sleep) (Blackwell et al., 2011) is a multicenter sleep cohort of older men (aged 65 years or older) that includes unattended in-home polysomnography (PSG), which was set up by trained technicians and annotated using standardized scoring procedures. The study was conducted between December 2003 and March 2005, during which 3,135 participants from the parent MrOS cohort of 5,994 men completed overnight unattended in-home PSG. The dataset available through the National Sleep Research Resource (NSRR) includes PSG recordings in European Data Format (EDF) and XML annotation files with multimodal biosignals, including EEG, EOG, EMG, ECG, nasal cannula (airflow), thoracic and abdominal respiratory effort, oxygen saturation, and body position. Respiratory event annotations were harmonized via rule-based post-processing of the original labels to ensure consistent criteria across datasets, and details are described in (Ahn et al., 2025). For the present study, we analyzed data from two sleep visits (Visit 1, 2003–2005; Visit 2, 2009–2012). We excluded recordings missing any of the required signals (EEG, EOG, EMG, ECG, airflow, thoracic/abdominal effort, or oxygen saturation). Of the 2,911 participants with successful PSG recordings, 2,678 (Visit 1) and 998 (Visit 2) were included in the final analytic cohort after quality control.

A.7. Institute of Systems and Robotics, University of Coimbra (ISRUC) Dataset

The Institute of Systems and Robotics, University of Coimbra (ISRUC) dataset (Khalighi et al., 2016) is a publicly available repository provided by the Sleep Medicine Center of the Hospital of Coimbra University (CHUC). The dataset is divided into three subgroups: SG1 and SG2, which feature patients with sleep disorders, and SG3, which consists of healthy control subjects. Each recording comprises 19 signals, including six EEG channels (F3-A2, C3-A2, O1-A2, F4-A1, C4-A1, O2-A1), dual-channel EOG and EMG, and various respiratory and cardiac sensors. Considering its relatively small size, this dataset is used to evaluate the adaptation efficiency of our model.

A.8. Demographics analysis

Figure 7 shows the age and BMI distribution stratified by sex based on our pretraining datasets.

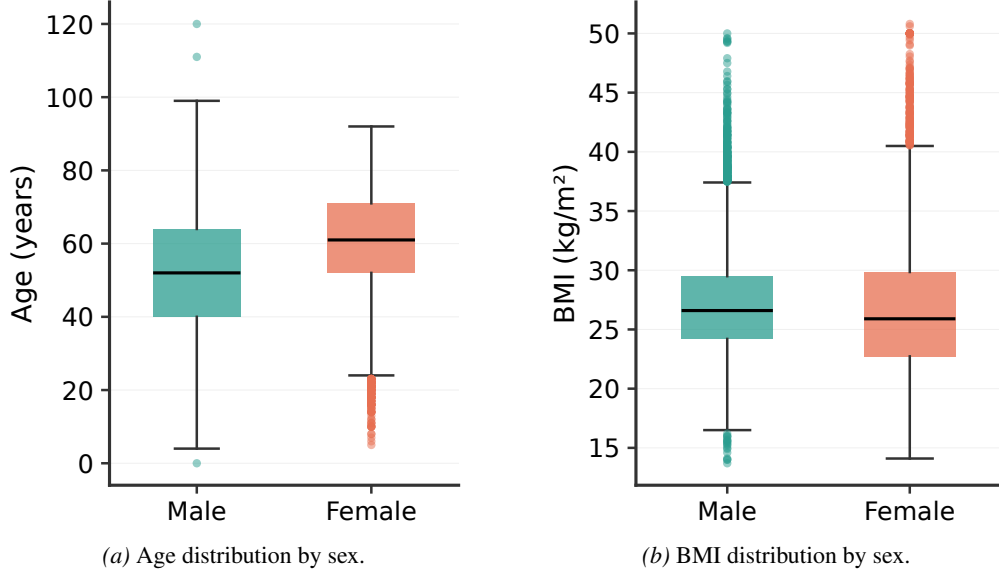


Figure 7. Demographic distributions of the pre-training dataset. (a) Age distribution shows a median of approximately 52 years for males and 61 years for females. (b) BMI distribution shows similar medians across sexes (approximately $27 \text{ kg}/\text{m}^2$ for males and $26 \text{ kg}/\text{m}^2$ for females), with notable outliers in both groups.

B. Model architecture details

Table 8 summarizes the specification of the Micro-Encoder and the Macro-Encoder.

Table 8. Architecture Specification for the Micro- and Macro- Encoders. Norm: Normalization layer (RMSNorm), Exp: Expansion convolution, DW: Depthwise convolution, PW: Pointwise convolution

Encoder	Module	Item	Dim.	Kernel	Stride	Depth	Heads	Notes
Micro	Private	Patch Emb.	Patch Emb. (Conv blocks)	[32,64,128]	[10,5,1]	[10,5,1]	–	Conv-Norm-GELU
		Transformer blocks (Lower)	128	–	–	2	8	
		Patch Merge	384	10	5	–	–	Exp-DW-Norm-PW-GELU-PW
	Shared	Transformer blocks (Higher)	384	–	–	2	8	
		MoE Transformer blocks	384	–	–	4	8	4 Experts, 2 Activated
		Transformer blocks	384	–	–	4	8	Cross-Attention
	Decoder	Upsample	128	–	–	–	–	
		Linear embedding	64	–	–	–	–	
		Transformer blocks	64	–	–	2	4	
		Projection (Linear)	50	–	–	–	–	Same as the patch size
Macro	Macro	Linear projection	512	–	–	–	–	
		Mamba blocks (Forward)	512	–	–	2	–	PreNorm-Mamba-PostNorm
		Mamba blocks (Backward)	512	–	–	2	–	PreNorm-Mamba-PostNorm

C. Training details

Pretraining is done in two-step process. The Micro-Encoder is trained in the first step and the Macro-Encoder is trained in the second step. Table 9 summarizes pretraining details for both Micro- and Macro-Encoder. When pretraining Macro-Encoder, we did not include PHY dataset because the dataset does not provide BMI information. Moreover, in other datasets, when the demographic attributes are not in proper format or unavailable, we exclude those records.

Table 10 summarizes the finetuning settings for downstream tasks used for Section 4.

When calculating the reconstruction loss for Micro-Encoder (\mathcal{L}_{Mi}^{recon}), the raw signal is smoothed using moving average of eleven adjacent points. This effectively eliminates noises and helps the model focus on more meaningful signals.

Table 9. Hyperparameter settings for pretraining for Micro and Macro-Encoders

Encoder	Item	Value	Notes
Micro-Encoder	Mask ratio	50%	
	Batch size	512	
	Input length	60 seconds	Equivalent to 120 epochs
	Optimizer	AdamW	
	β_1	0.9	
	β_2	0.99	
	Weight decay (λ)	0.05	
	Initial learning rate	5.00×10^{-4}	
	Learning rate schedule	Cosine annealing	
	Final learning rate	1.00×10^{-8}	
	Training epochs	3	
	Patch size	500 ms	Equivalent to 50 input points
	Temperature for contrastive loss (τ)	0.07	
	Sequence length for contrastive loss	30 seconds	
	Weight for contrastive loss (λ_{CL})	0.1	
	Weight for KoLeo loss (λ_{KoLeo})	0.01	
	Timespan for contrastive loss	30 seconds	Equivalent to 60 epochs
Macro-Encoder	Batch size	40	Subjects
	Maximum number of epochs per subject	1,080	Equivalent to 540 minutes
	Optimizer	AdamW	
	β_1	0.9	
	β_2	0.99	
	Weight decay (λ)	0.05	Not applied to SSM parameters
	Initial learning rate	1.00×10^{-4}	
	Learning rate schedule	Cosine annealing with warmup	
	Final learning rate	1.00×10^{-8}	
	Training epochs	4	
	Temperature for contrastive loss (ρ)	0.1	
	Temperature for weight calculation (v)	0.5	
	Cycle length	90 minutes	180 epochs
	Demographic distance for sex difference (λ_{sex})	1	

Table 10. Training details used for downstream tasks.

Downstream tasks	Item	Value	Notes
Sleep staging	Loss	Weighted Cross Entropy	$w_k = \log_5(N/N_k)$ for class k
	Initial learning rate	1.00×10^{-2}	
	Batch size	4	Subjects
Apnea segmentation	Loss	Weighted Cross Entropy	$w_k = N/N_k$ for class k
	Initial learning rate	4.00×10^{-4}	
	Batch size	1024	Epochs
Disease prediction	Loss	Cox PH	
	Initial learning rate	1.00×10^{-2}	
	Batch size	4	Subjects
Age / AHI estimation	Loss	MAE	
	Initial learning rate	1.00×10^{-2}	
	Batch size	4	Subjects
Sex classification	Loss	Cross Entropy	
	Initial learning rate	1.00×10^{-2}	
	Batch size	4	Subjects
Common settings	Optimizer	AdamW	
	β_1	0.9	
	β_2	0.99	
	Weight decay (λ)	1×10^{-4}	
	Learning rate schedule	Cosine annealing	
	Final learning rate	1.00×10^{-8}	
	Training epochs	3	

D. More experimental results

D.1. Ablation study

Table 11 summarizes the sleep staging performance improvement of our principal components. The performance is evaluated on the SHHS1 test split. Experiments 1-3 is pretrained on SHHS1 train split and experiments 4-5 are done using the entire pretraining datasets. Table 12 presents the sleep staging accuracy measured on SHHS1 test split with varying demographic factors used for DGCL. DGCL is only done for the training split of SHHS1.

Table 11. **Ablation Study of SleepMaMi Components.** We evaluate the contribution of each module and training strategy to the final sleep staging accuracy on the SHHS1 dataset.

Id	Private encoder	Shared encoder	MAE	CL	Large scale pretraining	DGCL	Acc. (%)
1	✓		✓				74.8
2	✓	✓	✓	✓			75.7
3	✓	✓	✓	✓	✓		76.0
4	✓	✓	✓	✓	✓		79.8
5	✓	✓	✓	✓	✓	✓	81.9

Table 12. **Ablation Study of Demographic Factors in DGCL.** We investigate the impact of different demographic supervisory signals—Age, Sex, and BMI—on the final sleep staging accuracy. DGCL is only done on SHHS1 training split.

Id	Age	Sex	BMI	Acc. (%)
1				79.8
2	✓			80.6
3		✓		80.2
4			✓	80.1
5	✓	✓	✓	80.7

D.2. Sleep macro-structure analysis

To further investigate the demographic and clinical factors that influence sleep stage distributions, we present extended visualizations across various subgroups. Figure 8 shows sleep stage distributions by sex combined with age group, BMI category, and sleep apnea severity (AHI), respectively. Figure 9 presents the interactions between non-sex factors, revealing how multiple variables jointly influence sleep stage distributions throughout the night.

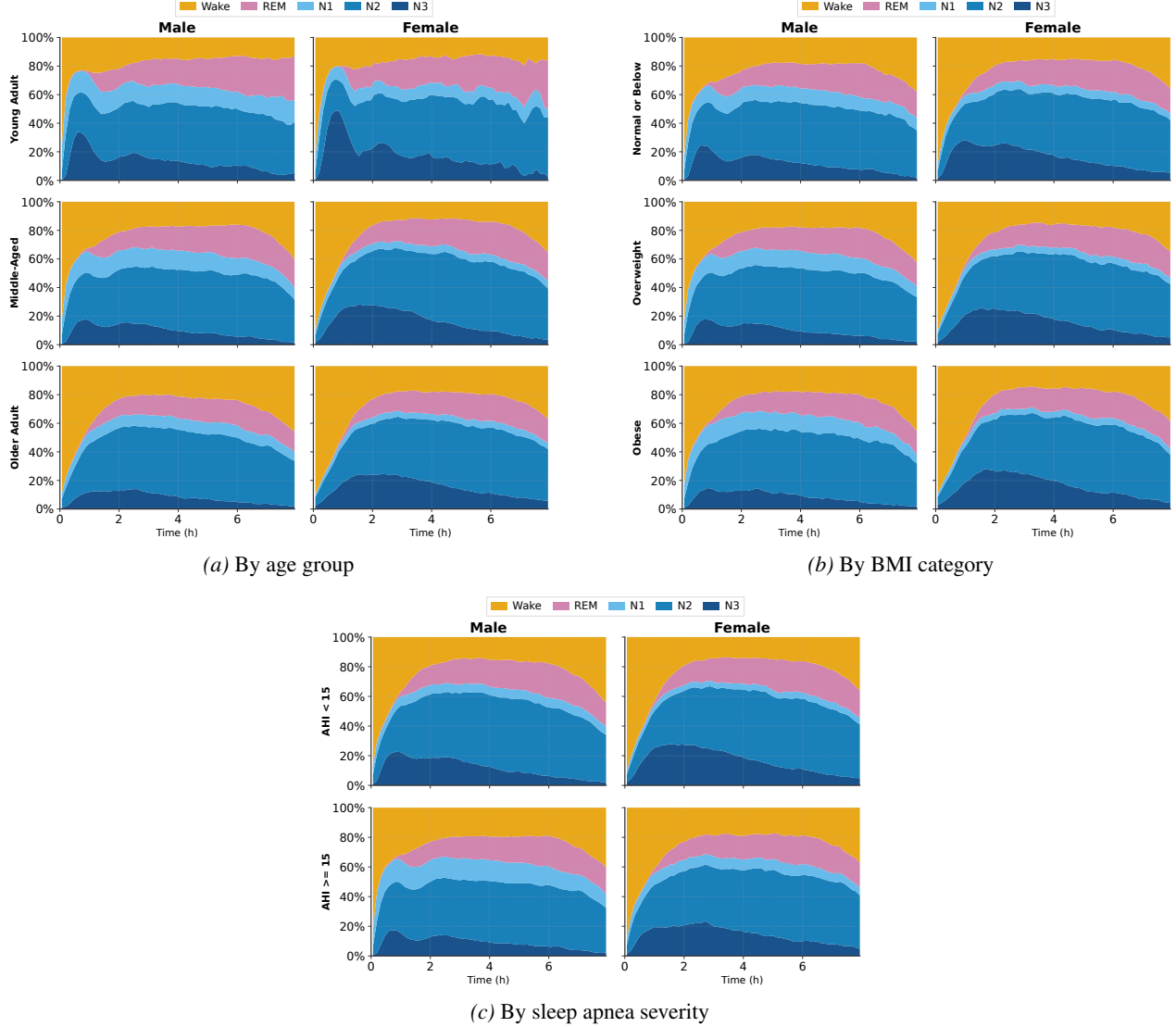
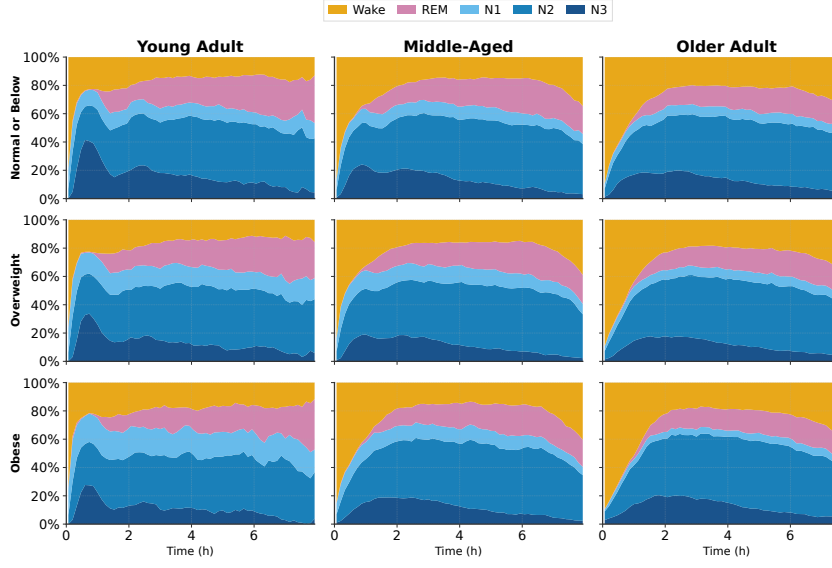
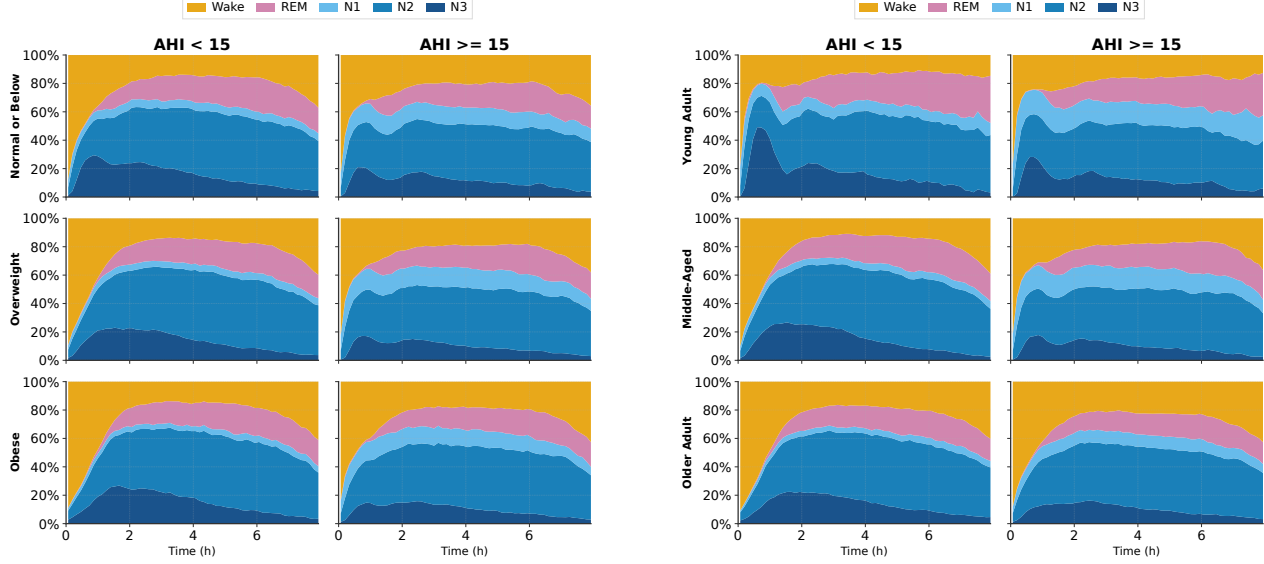


Figure 8. Sleep macrostructure variations across demographic and clinical groups. (a) Age groups: Young Adult (18–44 years), Middle-Aged (45–64 years), Older Adult (≥ 65 years). (b) BMI categories: Normal or Below ($< 25 \text{ kg/m}^2$), Overweight (25–30 kg/m^2), Obese ($\geq 30 \text{ kg/m}^2$). (c) Sleep apnea severity based on Apnea-Hypopnea Index (AHI ≥ 15 events/h indicates moderate-to-severe). These demographic-dependent patterns motivate our Demographic-Guided Contrastive Learning objective.



(a) By BMI and age group



(b) By BMI and AHI

(c) By age group and AHI

Figure 9. Sleep macro-structure variations across combined demographic and clinical factors. (a) BMI categories (Normal or Below: $< 25 \text{ kg/m}^2$, Overweight: $25\text{--}30 \text{ kg/m}^2$, Obese: $\geq 30 \text{ kg/m}^2$) and age groups (Young Adult: 18–44 years, Middle-Aged: 45–64 years, Older Adult: ≥ 65 years). (b) BMI categories and sleep apnea severity (AHI < 15 vs. AHI ≥ 15 events/h). (c) Age groups and sleep apnea severity. These combined factors jointly influence sleep stage distributions throughout the night.

D.3. More embedding analysis

Figure 10 presents more visualizations of Macro-embeddings similar to those presented in Figure 6 using different demographic features.

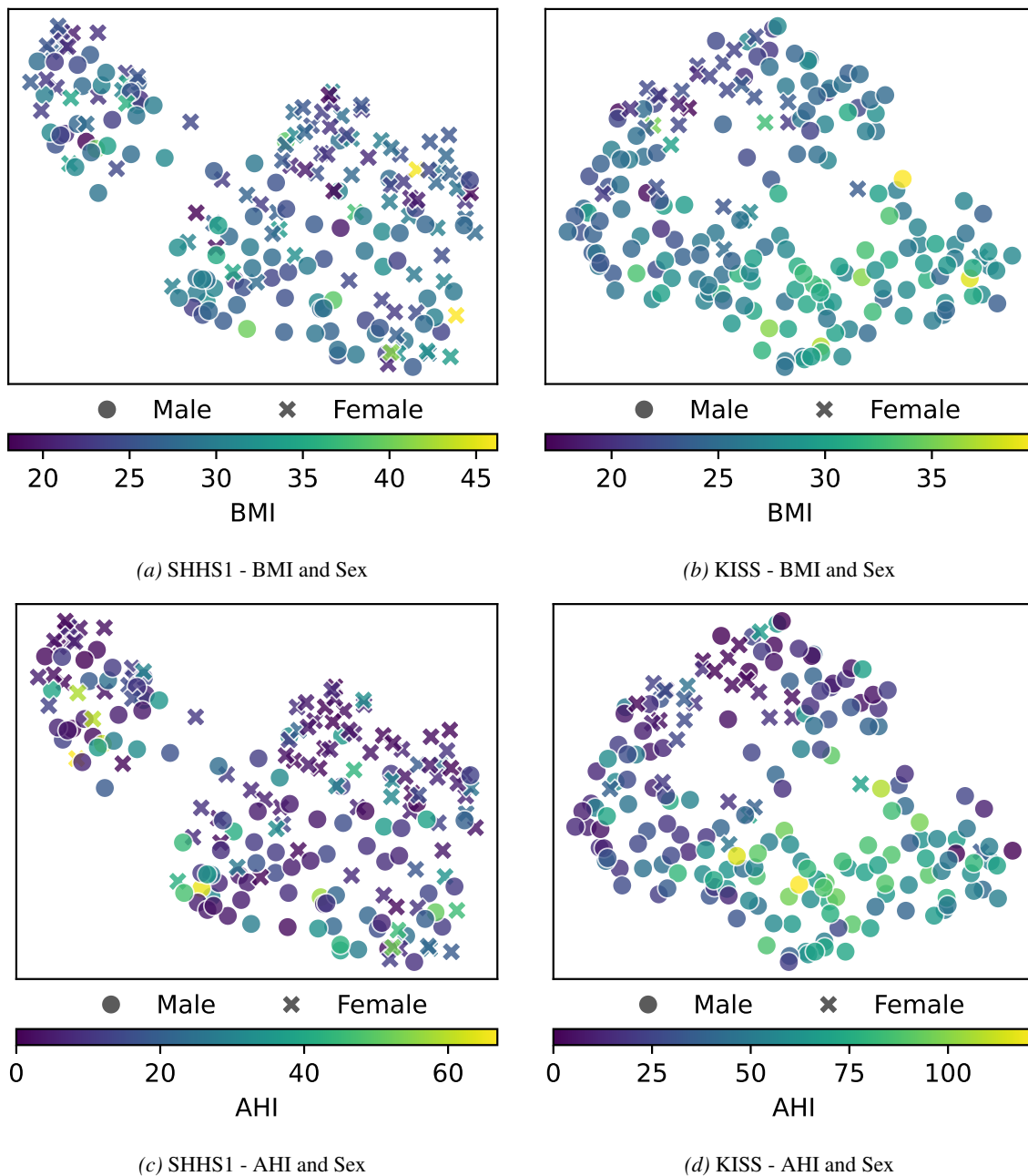


Figure 10. Macro-embeddings visualization. Per-subject latent embeddings from Macro-Encoder is visualized using U-MAP. Each point represents a single subject's embeddings where color and symbol represents demographic characteristics.

D.4. Confusion matrix

In Figure 11, we provide the confusion matrix for sleep staging and SDB segmentation evaluated on the test split of SHHS1 and KISS.

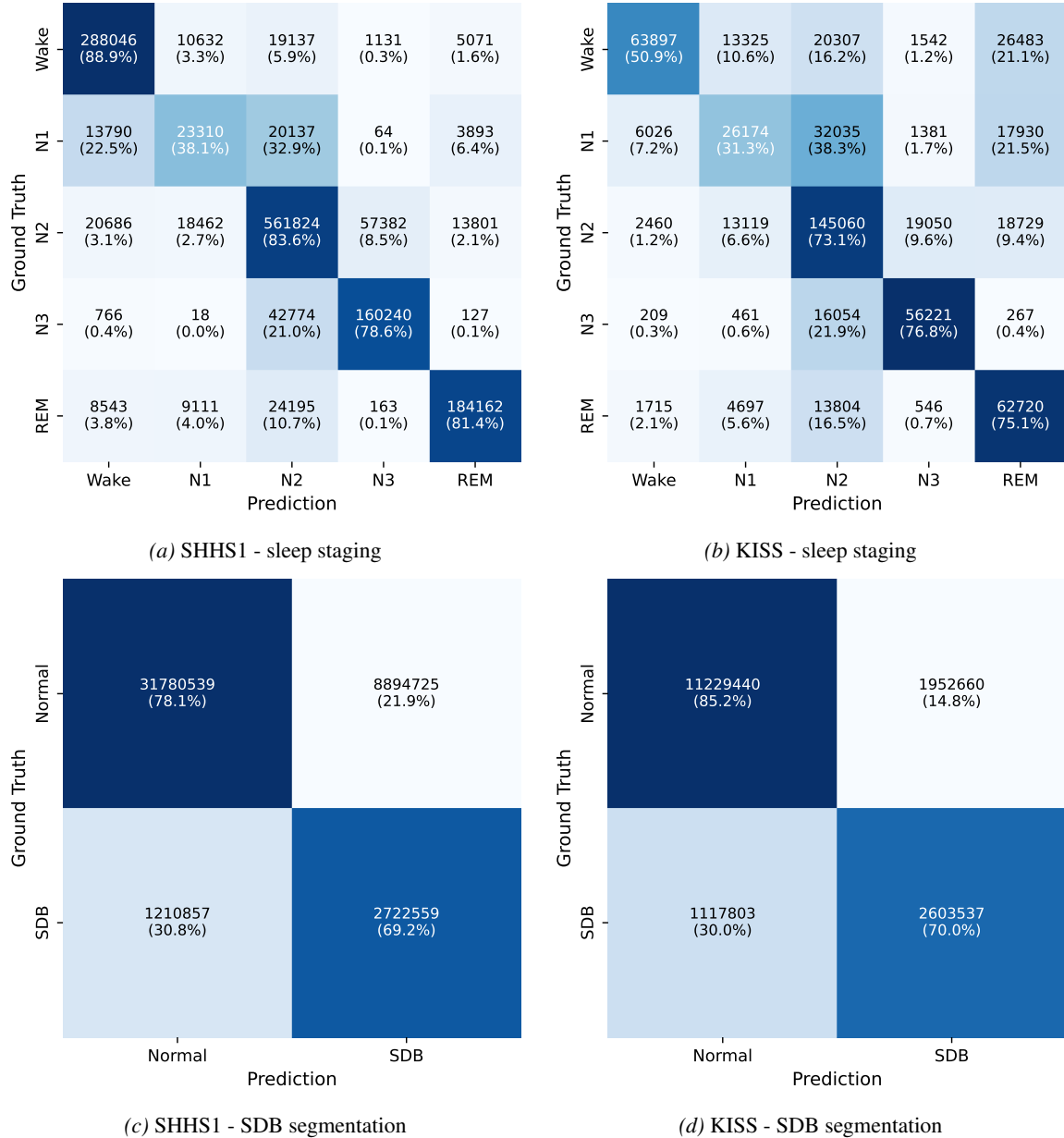


Figure 11. Confusion matrix for sleep staging and SDB segmentation on the test split of SHHS1 and KISS.